J. Fluid Mech. (2001), *vol.* 447, *pp.* 31–51.
DOI: 10.1017/S0022112001005535 Printed in the United Kingdom

Transverse waves in numerical simulations of cellular detonations

By GARY J. SHARPE

School of Mathematics and Statistics, University of Birmingham, Edgbaston, Birmingham B15 2TT, UK

(Received 19 July 2000 and in revised form 4 May 2001)

In this paper the structure of strong transverse waves in two-dimensional numerical simulations of cellular detonations is investigated. Resolution studies are performed and it is shown that much higher resolutions than those generally used are required to ensure that the flow and burning structures are well resolved. Resolutions of less than about 20 numerical points in the characteristic reaction length of the underlying steady detonation give very poor predictions of the shock configurations and burning, with the solution quickly worsening as the resolution drops. It is very difficult and dangerous to attempt to identify the physical structure, evolution and effect on the burning of the transverse waves using such under-resolved calculations. The process of transverse wave and triple point collision and reflection is then examined in a very high-resolution simulation. During the reflection, the slip line and interior triple point associated with the double Mach configuration of strong transverse waves become detached from the front and recede from it, producing a pocket of unburnt gas. The interaction of a forward facing jet of exploding gas with the emerging Mach stem produces a new double Mach configuration. The formation of this new Mach configuration is very similar to that of double Mach reflection of an inert shock wave reflecting from a wedge.

1. Introduction

A detonation is a rapid regime of burning in which a strong shock ignites the fuel and the burning proceeds to equilibrium behind the shock, while the energy released continues to help to drive the shock. Experiments (see, for example, Fickett & Davis 1979) reveal that detonation fronts usually have a complicated three-dimensional, time-dependent structure with interior transverse shock waves. Perhaps of most interest are the cellular detonations that appear in rectangular tubes. In these cases the leading shock is wrinkled, consisting of alternate weak incident shocks and stronger Mach stems, joined at triple points by transverse waves which travel back and forth perpendicular to the front and extend back into the reaction zone. If soot is deposited on the walls of the tube then the tracks of these triple points can map out the boundaries of 'cells', which can be remarkably regular diamond shapes. The characteristic size of the cells and the degree of regularity depends on the composition of the fuel and the initial conditions (Strehlow 1969), but they are usually one to two orders of magnitude greater than the underlying steady, one-dimensional detonation reaction length (Lee 1984). Two distinct types of transverse shock wave are seen in the experiments (Fickett & Davis 1979). Transverse waves of the *weak* type consist of a single, simple shock wave which extends back into the flow from the triple point on the shock front. *Strong* transverse waves, however, are kinked at a second triple

point inside the reaction zone, and a portion of the transverse wave downstream of this triple point is itself a detonation. This detonation portion of the main transverse shock can have its own transverse waves moving back and forth along it.

Many numerical simulations of cellular detonations and transverse wave structures have been performed. Both the strong and weak types of transverse shock waves are seen in such simulations (Bourlioux & Majda 1992; Quirk 1994; Lefebvre & Oran 1995; Sharpe & Falle 2000*a*). The majority of unstable detonation simulations have used a single, irreversible reaction with an Arrhenius form of the reaction rate, and a polytropic equation of state. While this idealized model can be criticized on the grounds that it ignores the complexity of real chemistry, it is clearly essential to first establish that this simple case can be computed reliably (Quirk 1994; Sharpe & Falle 2000*a*, *b*) before trying to simulate detonations with realistic chemistry involving multiple species and reaction length scales. Even with this simple detonation model, the simulations are in remarkable qualitative agreement with the experiments. In the idealized model, the presence of weak transverse waves is associated with small heat release (Bourlioux & Majda 1992), or with small cells seen in the initial stages of the development of the instability or in very narrow tubes (Sharpe & Falle 2000*a*). In the fully developed cells for moderate to large heat release the transverse waves are of the strong type.

Experience has shown that if one wishes to reveal the correct time-dependent physics of detonations using numerical simulations then it is essential to perform resolution studies. For the simpler one-dimensional, or pulsating, instability over 50 mesh points in the half-reaction length of the underlying steady, planar detonation are required to obtain acceptable solutions for the idealized detonation model, while over 100 points are required to obtain a truly converged solution (Sharpe & Falle 2000*b*). Resolutions of less than about 20 points per half-reaction length give very poor or else entirely spurious solutions. Short & Quirk (1997) have shown that for pulsating detonations with realistic chain-branching reactions, a few hundred points per half-reaction length may be required to obtain even the qualitatively correct solutions. The resolution required to obtain converged solutions in multi-dimensional cellular detonation simulations is likely to be higher than that for the simpler pulsating detonations.

Resolution studies of two-dimensional numerical simulations show that below about 20 points per half-reaction length, the evolution, size and regularity of the detonation cells, produced by the motion of the transverse waves and triple points, are grid dependent (Sharpe & Falle 2000*a*). Although Sharpe & Falle (2000*a*) did not investigate the transverse waves in depth, they did show that the shock configurations were not well resolved at these resolutions.

In this paper we investigate the nature of strong transverse waves in numerical simulations of cellular detonations. Thorough resolution studies of a complex strong transverse wave are first performed. Such resolution studies also provide a benchmark so that the results of different numerical schemes can be compared at different resolutions, with the hope that a consensus can be achieved as to what constitutes a correct solution, and which are the most suitable numerical schemes. We then investigate the collision of transverse waves and triple points in a very high-resolution simulation.

The plan of the paper is as follows: the governing equations are given in § 2; the numerical method is discussed in § 3; the results of the resolution study are given in § 4; triple point collision is investigated in § 5; the results are compared to those of experiments and previous calculations in § 6; § 7 contains the conclusions and suggestions for future work.

2. Governing equations

In two dimensions, the governing equations for our idealized detonation are

$$\left.\begin{gathered}\frac{\partial\rho}{\partial t}+\frac{\partial(\rho u)}{\partial x}+\frac{\partial(\rho v)}{\partial y}=0,\quad \frac{\partial(\rho u)}{\partial t}+\frac{\partial(p+\rho u^2)}{\partial x}+\frac{\partial(\rho uv)}{\partial y}=0,\\ \frac{\partial(\rho u)}{\partial t}+\frac{\partial(\rho uv)}{\partial x}+\frac{\partial(p+\rho v^2)}{\partial y}=0,\quad \frac{\partial E}{\partial t}+\frac{\partial(Eu+pu)}{\partial x}+\frac{\partial(Ev+pv)}{\partial y}=0,\\ \frac{\partial(\rho\lambda)}{\partial t}+\frac{\partial(\rho u\lambda)}{\partial x}+\frac{\partial(\rho v\lambda)}{\partial y}=W,\end{gathered}\right\} \tag{2.1}$$

where u and v are the components of the fluid velocity in the laboratory frame, in the x- and y-directions respectively, ρ the density, p the pressure, E the total energy per unit volume, λ the reaction progress variable (with $\lambda = 1$ for unburnt and $\lambda = 0$ for burnt) and $W \equiv W(\rho, p, \lambda)$ the reaction rate. We assume an Arrhenius form of the reaction rate and a perfect gas, so that

$$E = \frac{p}{\gamma - 1} + \tfrac{1}{2}\rho u^2 - \rho q(1-\lambda) \tag{2.2}$$

and

$$W = -\alpha\rho\lambda \mathrm{e}^{-\tau/T}, \tag{2.3}$$

with

$$T = \frac{p}{\rho}, \tag{2.4}$$

where q is the (constant) heat of reaction, γ the (constant) ratio of specific heats, T the temperature, τ the activation temperature, and α a constant rate coefficient.

These equations have been non-dimensionalized by using the upstream density, the steady, planar detonation speed and the half-reaction length in the steady wave, i.e. the distance between the shock and the point where $\lambda = 1/2$ (see, for example, Sharpe 1997). These scalings have the advantage that both the half-reaction length and half-reaction time of the steady detonation are unity in the dimensionless variables. The only parameter left to vary in the upstream state is the non-dimensional pressure

$$p_- = \frac{\bar{p}_-}{\bar{\rho}_- \bar{D}^2}, \tag{2.5}$$

where the bar denotes dimensional quantities, the minus subscript denotes quantities in the upstream, quiescent state and $\bar{D}$ is the steady, planar detonation speed.

Various other scalings are widely used. In most numerical simulations of the idealized detonation the activation temperature and heat of reaction are scaled with the upstream temperature, $\bar{T}_-$. The values of activation temperature and heat of reaction, E and Q, in these scales are then related to ours by

$$E = \frac{\tau}{p_-}, \quad Q = \frac{q}{p_-}. \tag{2.6}$$

Another scaling used is to non-dimensionalize the activation temperature and heat of reaction with the post-shock temperature in the steady, planar wave, $\bar{T}_s$. The dimensionless activation temperature and heat of reaction using this scaling, θ and β, are related to ours by

$$\theta = \frac{\tau}{T_s}, \quad \beta = \frac{q}{T_s}, \tag{2.7}$$

where

$$T_s = \frac{(1 - 2\gamma p_- - \gamma)(\gamma p_- - p_- - 2)}{(\gamma + 1)^2}. \tag{2.8}$$

In this paper, unless otherwise specified, we use the same parameter set as Sharpe & Falle (2000*a*), i.e. the Chapman–Jouguet detonation with $E = 20$, $q = 50$ and $\gamma = 1.2$. This corresponds to values of $\tau = 0.431$, $p_- = 0.0216$ (giving $q = 1.078$) and $\theta = 4.16$, $\beta = 10.38$. For these parameters the planar detonation is stable to one-dimensional (longitudinal) perturbations and has a simple band of linearly unstable wavelengths in the transverse direction (Sharpe & Falle 2000*a*).

3. Numerical method

3.1. *Numerical code*

In this paper we use the hierarchical adaptive code, μCobra, which has been developed for industrial applications by Mantis Numerics Ltd, and is described in Falle & Giddings (1993) and Falle (1991), but for the sake of completeness it is worth summarizing its main features here. It is a second-order Godunov scheme in which the second-order Riemann problems are constructed from the primitive variables using a quadratic averaging function. An exact Riemann solver is used wherever necessary and a linear solver elsewhere. Second-order artificial dissipation is added to the fluxes determined from the Riemann solution in order to suppress the Quirk instability (Quirk 1992) and to remove the entropy oscillations behind slowly moving shocks. The form of this additional dissipation is described in Falle & Komissarov (1996). The code uses a hierarchical series of Cartesian grids $G^0, \ldots, G^N$, so that grid G^n has mesh spacing $h/2^n$, where h is the mesh spacing on the base grid G^0. Grids G^0 and G^1 cover the entire domain, but the higher grids only occupy regions where increased resolution is required. Refinement is controlled by comparing the solution of each conserved variable and also their rates of change on grids G^n and G^{n-1}. If either of these errors is greater than given tolerances then the grid is refined to level G^{n+1}, $n + 1 \leqslant N$. These conditions can be used to ensure that regions where the flow is changing rapidly, e.g. shocks, and to some extent the reaction zone, are always resolved to the highest level. However to ensure that the flow is always resolved wherever the reactions are occurring, we refine to the highest level whenever

$$|W| > \epsilon_1 \tag{3.1}$$

and whenever

$$\lambda > \epsilon_2 \quad \text{and} \quad p > 2p_-, \tag{3.2}$$

where W is the reaction rate and ϵ_1 and ϵ_2 are small. We take $\epsilon_1 = 0.01$ and $\epsilon_2 = 0.1$. Note that in the steady wave, (3.1) fully refines the reaction zone from the shock to a point where $\lambda \sim 0.01$, so that condition (3.2) may seem redundant. However (3.2) ensures that long induction zones, where the reaction rate is very low, but the fuel is unburnt, do not become derefined.

In this paper, unless otherwise specified, we use a base grid with spacing of 1 point per half-reaction length and 2 to 5 refinement levels, giving effective resolutions of 4, 8, 16, 32 and 64 points per half-reaction length (points/$l_{1/2}$).

3.2. *Initial and boundary conditions*

In our simulations the detonation runs from left to right in the positive x-direction. Since the fluid ahead of the detonation is in its quiescent state, this means that the

right-hand boundary condition is irrelevant provided the shock remains with the domain. As discussed in Sharpe & Falle (1999), the left-hand boundary condition is somewhat more difficult. We therefore place the left boundary at $x = -100$ and impose a zero-gradient condition. This is far enough behind the initial position of the front to ensure that it has little effect during the calculation. The boundary conditions imposed on the upper and lower boundaries are symmetry conditions, so that these boundaries correspond to either planes of symmetry or solid, reflecting walls. The domain width in the y-direction is 10 in § 4 and § 5, while there is a calculation with width 5 in § 6. We consider one transverse wave (i.e. half a cell) in the domain which reflects from the $y = 0$ and $y = L$ boundaries, where L is the width of the domain, producing a cell size of $2L$. For the calculations in § 4 and § 5, this is close to the natural cell size, which is between 20 and 30 for the parameter set used (Sharpe & Falle 2000*a*), while the domain width is narrow enough to allow very high resolution.

The initial data are given by placing the steady, one-dimensional detonation on the grid in the region $x < 0$, with the plane shock lying along $x = 0$ and moving to the right. The one-dimensional detonation is then perturbed by placing a disturbance in the ambient density between $x = 0$ and $x = 1$. This perturbation, ρ', has the form

$$\rho' = \begin{cases} 0, & x < 0 \\ 0.25[1 + \cos(\pi y/L)] \sin(\pi(1 - x)), & 0 \leqslant x \leqslant 1 \\ 0, & x > 1, \end{cases}$$

i.e. a half-sinewave profile in the x-direction and a sinusoidal profile in the y-direction with amplitude 0.5 and wavelength $2L$, where L is the width of the domain. This perturbation quickly stimulates the formation of a single transverse wave, or half a cell, across the tube.

The detonation is then allowed to run for 10 cell lengths, or some 400 half-reaction lengths or times, to ensure that the solution is free from initial transients and that the transverse wave has reached full strength and settled into a regular, repeating pattern of reflections from the transverse boundaries.

While this paper is not about the best or most efficient numerical scheme for performing unstable detonation calculations, for purposes of comparison with other numerical schemes, it is worthwhile to give an indication of the computational cost when using μCobra. For the calculation with a resolution of 64 points/$l_{1/2}$ and domain width 10 presented in § 4 and § 5, to propagate the detonation one cell length (once the instability was fully developed) took about 45 CPU hours on a Compaq DS20E.

3.3. *Diagnostics*

In order to determine the position and structure of the transverse shock waves and other regions of rapid change in the flow (shocks, contacts, slip lines), two-dimensional greyscale plots of the density and pressure gradient,

$$|\nabla\rho| = \left[\left(\frac{\partial\rho}{\partial x}\right)^2 + \left(\frac{\partial\rho}{\partial y}\right)^2\right]^{1/2}, \quad |\nabla p| = \left[\left(\frac{\partial p}{\partial x}\right)^2 + \left(\frac{\partial p}{\partial y}\right)^2\right]^{1/2}, \tag{3.3}$$

are shown. Since only the density changes rapidly across contacts and slip lines, whereas both pressure and density change rapidly in a shock, by combining plots of the pressure and density gradients, one can then distinguish between shocks and slip lines. In order to determine the reaction lengths and regions of burning, greyscale plots of both the reaction progress variable, λ, and the magnitude of the reaction rate, $|W|$, which is proportional to the rate of heat release, are shown.

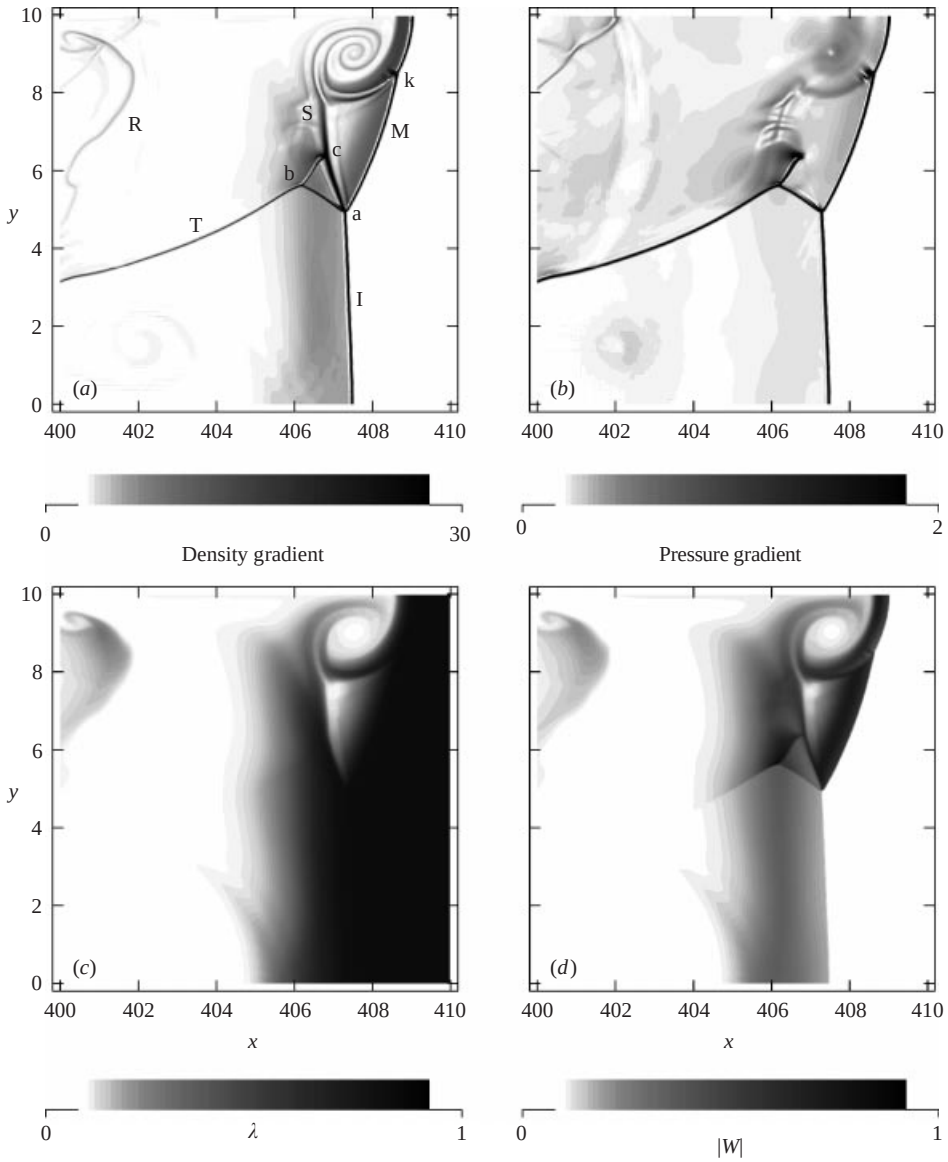

FIGURE 1. (*a*) Density gradient, (*b*) pressure gradient, (*c*) reaction progress variable and (*d*) reaction rate behind the front at $t = 408.1$ for a resolution of 64 points/$l_{1/2}$. I is the incident shock, M is the Mach stem, T is the transverse shock wave, S and R are slip lines, a and b are triple points, k is a kink in the Mach stem, c is the intersection of a shock with the slip line S.

4. Resolution studies

Figure 1 shows the density and pressure gradients, the reaction progress variable and reaction rate for the highest resolution used of 64 points/$l_{1/2}$ at $t = 408.1$. At this time the transverse wave is at a point in the cycle of reflections from the boundaries such that the triple point on the leading shock is halfway across the domain. The flow and reaction structures behind the front are quite complex. The origins of the various structures are discussed in § 5, here we will simply describe them. They are labelled in figure 1(*a*) as follows: I is the incident shock; M is the Mach stem, which is kinked

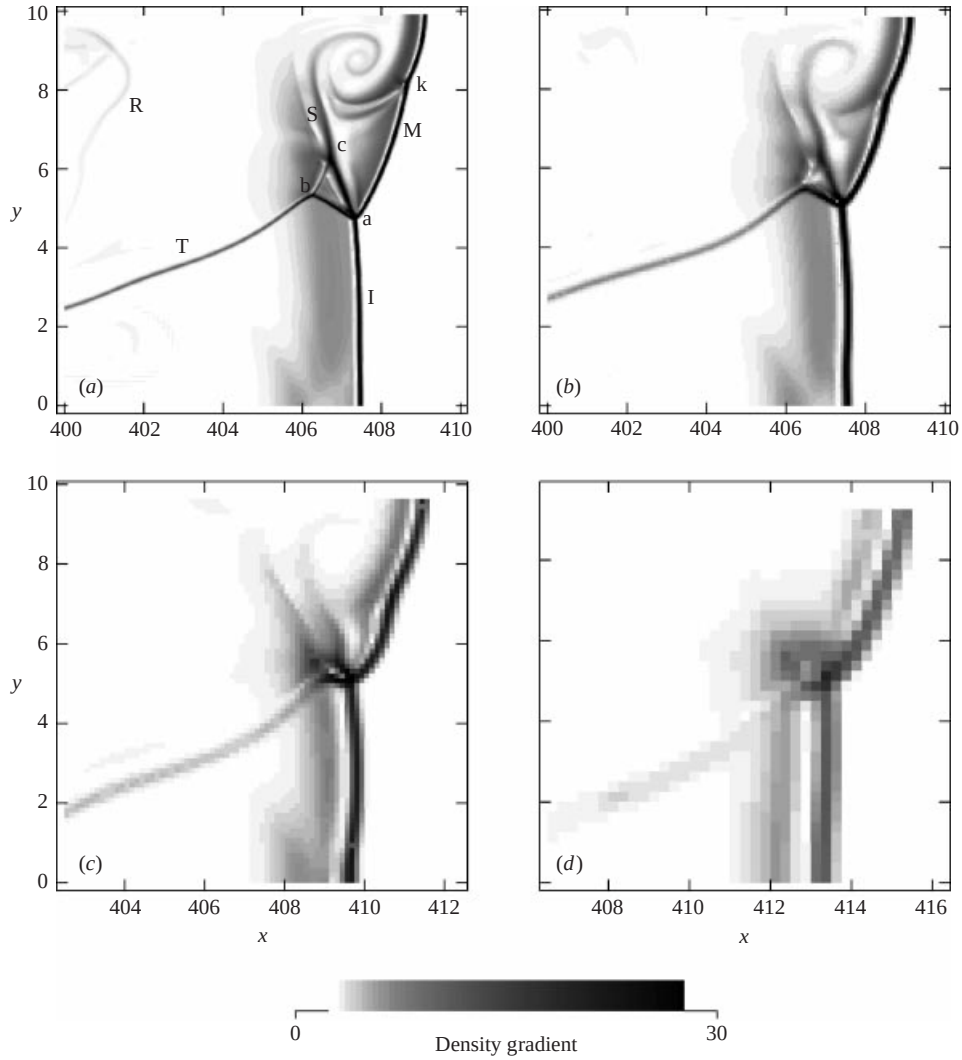

FIGURE 2. Density gradient for resolutions of (*a*) 32, (*b*) 16, (*c*) 8 and (*d*) 4 points/$l_{1/2}$.

at point k; T is the main transverse shock wave, which is travelling down and to the right; points a and b are triple points where three shocks join; S is a slip line which separates a region of completely burnt fuel which has passed through the Mach stem from a region of unburnt fuel which has passed through the incident shock. This slip line originates at the triple point a and then rolls up near the upper boundary. Another slip line, R, separates a pocket of burning gas located quite far behind the front from completely burnt fuel. The segment bc is a shock which terminates at point c on the slip line S. Note that the reaction rate is much higher behind the Mach stem than behind the incident shock, resulting in much shorter reaction length scales. One reason why very high resolution is required in numerical simulations of unstable detonations is that very disparate and changing reaction length scales occur. The reaction lengths are at times much shorter than in the steady wave and hence the number of points in the steady reaction length tells one very little about the resolution that will be required to properly resolve the shortest reaction lengths that

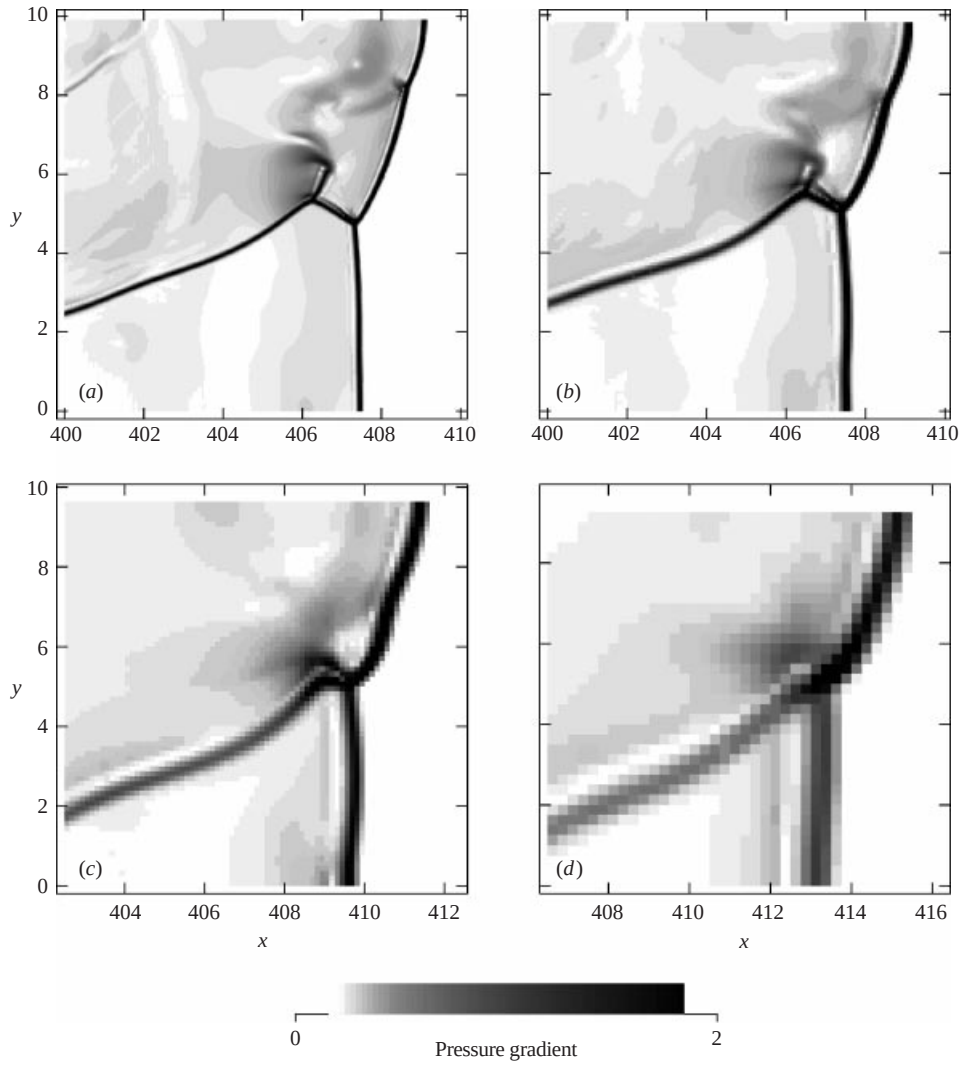

FIGURE 3. Pressure gradient for resolutions of (*a*) 32, (*b*) 16, (*c*) 8 and (*d*) 4 points/$l_{1/2}$.

appear in the unsteady flow. The reaction rate is highest behind the transverse shock near triple point b. The shock bc and part of the transverse shock T are moving through a region of unburnt fuel and hence raise the temperature and reaction rate in this fuel, acting like detonations themselves.

Figures 2–5 show the density gradient, the pressure gradient, the reaction progress variable and the reaction rate respectively, at the same point in the cycle of transverse wave reflections as for figure 1. In each of the figures, the results for resolutions of (*a*) 32, (*b*) 16, (*c*) 8 and (*d*) 4 points/$l_{1/2}$ are shown. It can be seen from figures 1–5 that there is a convergence of the features of the flow as the resolution increases.

For 32 points/$l_{1/2}$ all the structures described above for the higher resolution of 64 points/$l_{1/2}$ are present and in good agreement, although the roll-up of the slip line S is somewhat different. Hence we can have some confidence that the resolution of 64 points/$l_{1/2}$ constitutes at least a qualitatively very good solution for this parameter set, and all the salient features have been well resolved.

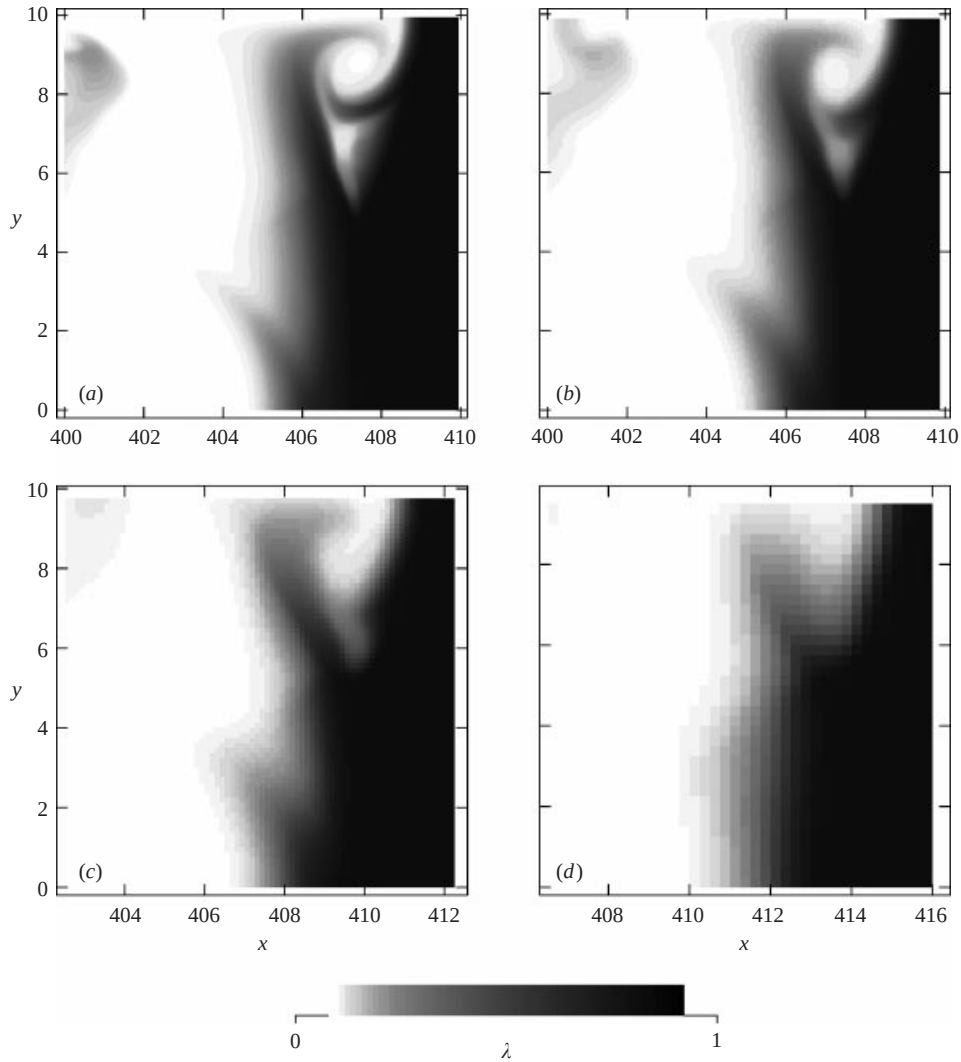

FIGURE 4. Reaction progress variable for resolutions of (*a*) 32, (*b*) 16, (*c*) 8 and (*d*) 4 points/$l_{1/2}$.

While at first glance 16 points/$l_{1/2}$ also appears to be in qualitative agreement with the more resolved calculations, without the context of the higher resolution results it would be quite difficult to correctly identify the flow features. For example, the kink in the Mach stem is not well defined and shock bc is not apparent in the density gradient. At times when the flow is more complex and involves finer details than for that in figures 1–5, i.e. shortly after the triple point reflects from a boundary, this resolution gives even poorer agreement with the higher resolved solutions (see § 6). Indeed, the details and mechanisms of the triple point collisions investigated in § 5 cannot be correctly elucidated by such resolutions. This resolution is also not enough to obtain the correct long-time cell sizes in wider domains (Sharpe & Falle 2000*a*).

Both 8 and 4 points/$l_{1/2}$ give very poor solutions for the shock structures and the burning. The double Mach point configuration is now not readily identifiable; indeed for 4 points/$l_{1/2}$ the transverse wave looks more like an unkinked weak transverse

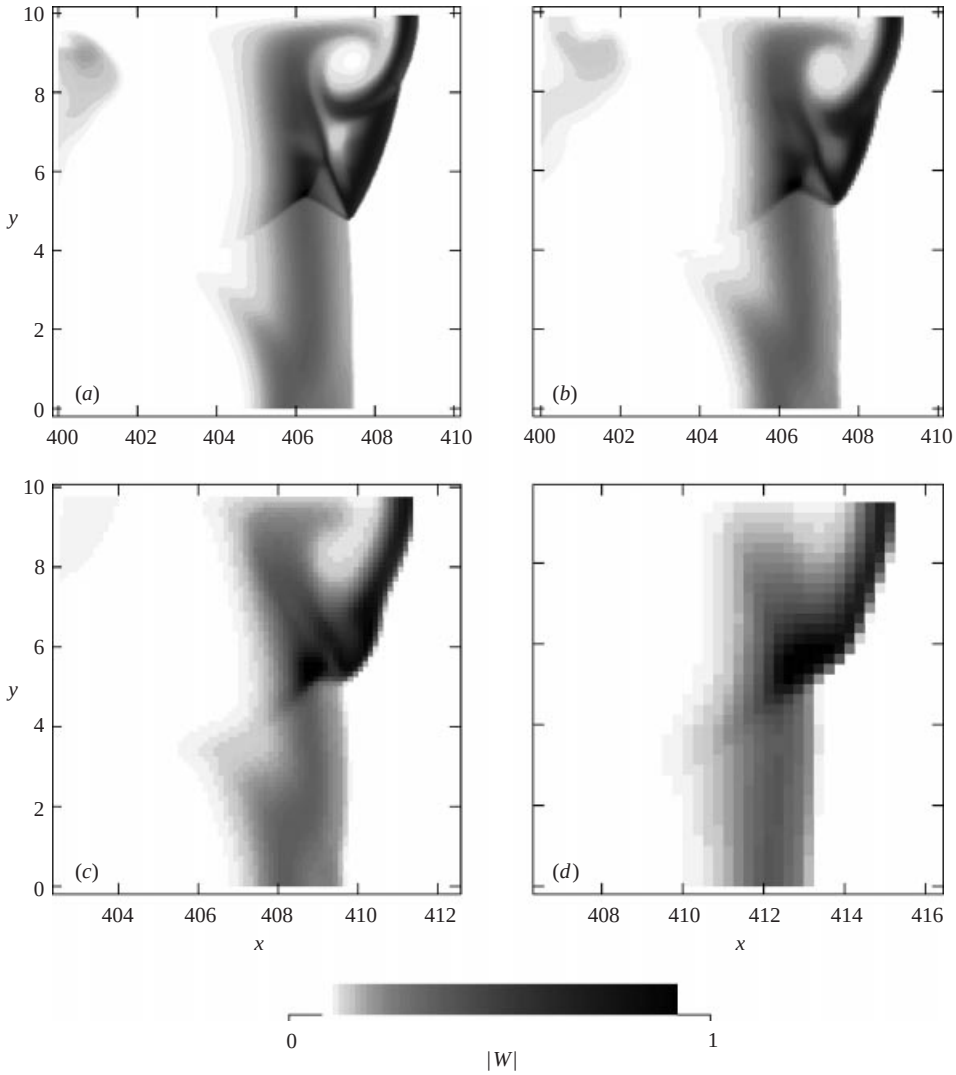

FIGURE 5. Reaction rate for resolutions of (*a*) 32, (*b*) 16, (*c*) 8 and (*d*) 4 points/$l_{1/2}$.

wave with a single triple point on the front. The nature of the burning is also quite wrong. The reaction, and hence heat release, rate is much higher in larger regions near the triple points than for the higher resolved solutions. Note that as the resolution decreases, the rate at which the pocket of unburnt gas behind the slip line R burns increases. For 8 and 4 points/$l_{1/2}$ the pocket is almost completely burnt out. Hence lower resolutions dramatically underestimate the increase in the effective burning length caused by such pockets falling behind the front. Finally, note that for these resolutions the cycle of transverse wave reflections from the boundaries is quite out of phase with the higher resolutions cases.

Even for this not too unstable case, it appears that more than 50 points/$l_{1/2}$ are required to ensure one is correctly capturing all the salient details. For resolutions of less than about 20 points/$l_{1/2}$ it becomes very difficult to identify the flow structures and motion without the benefit of a thorough resolution study, and the solution

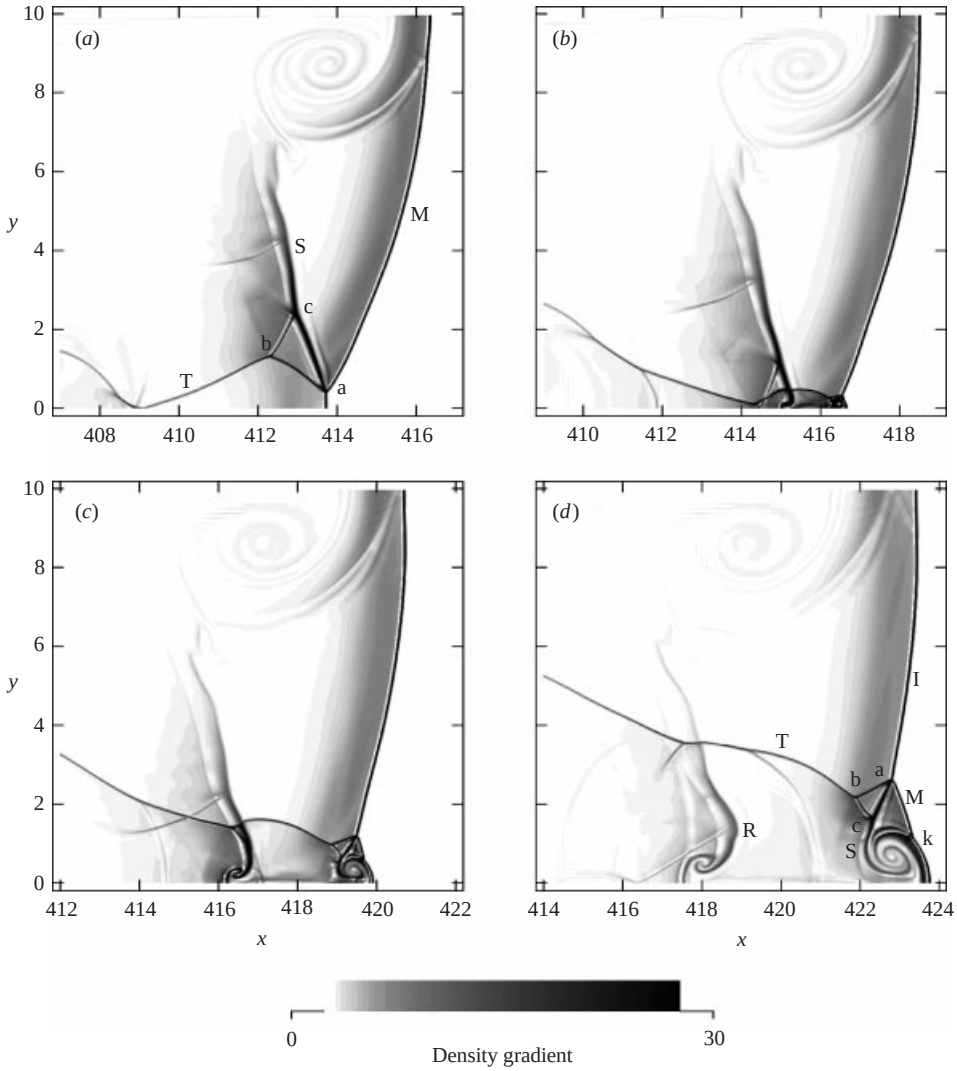

FIGURE 6. Density gradient for a resolution of 64 points/$l_{1/2}$ at times (*a*) 415.4, (*b*) 417.8, (*c*) 420.3 and (*d*) 423.3.

quickly becomes worse as the resolution drops. Figures 1–5 show that it is extremely dangerous to try and interpret anything about the correct physics from such under-resolved calculations.

5. Transverse wave and triple point collision

In this section, the process of transverse wave and triple point collision and reflection is investigated. Figures 6–9 show the density gradient, pressure gradient, reaction progress variable and reaction rate respectively at times (*a*) 415.4, (*b*) 417.8, (*c*) 420.3 and (*d*) 423.3, when the resolution is 64 points/$l_{1/2}$. Some extra features, not readily apparent at the earlier time of $t = 408.1$ corresponding to figure 1, are labelled in figure 7(*a*). W is a relatively weak shock wave which is propagating downwards through the unburnt fuel behind the slip line S, raising the reaction rate behind it and

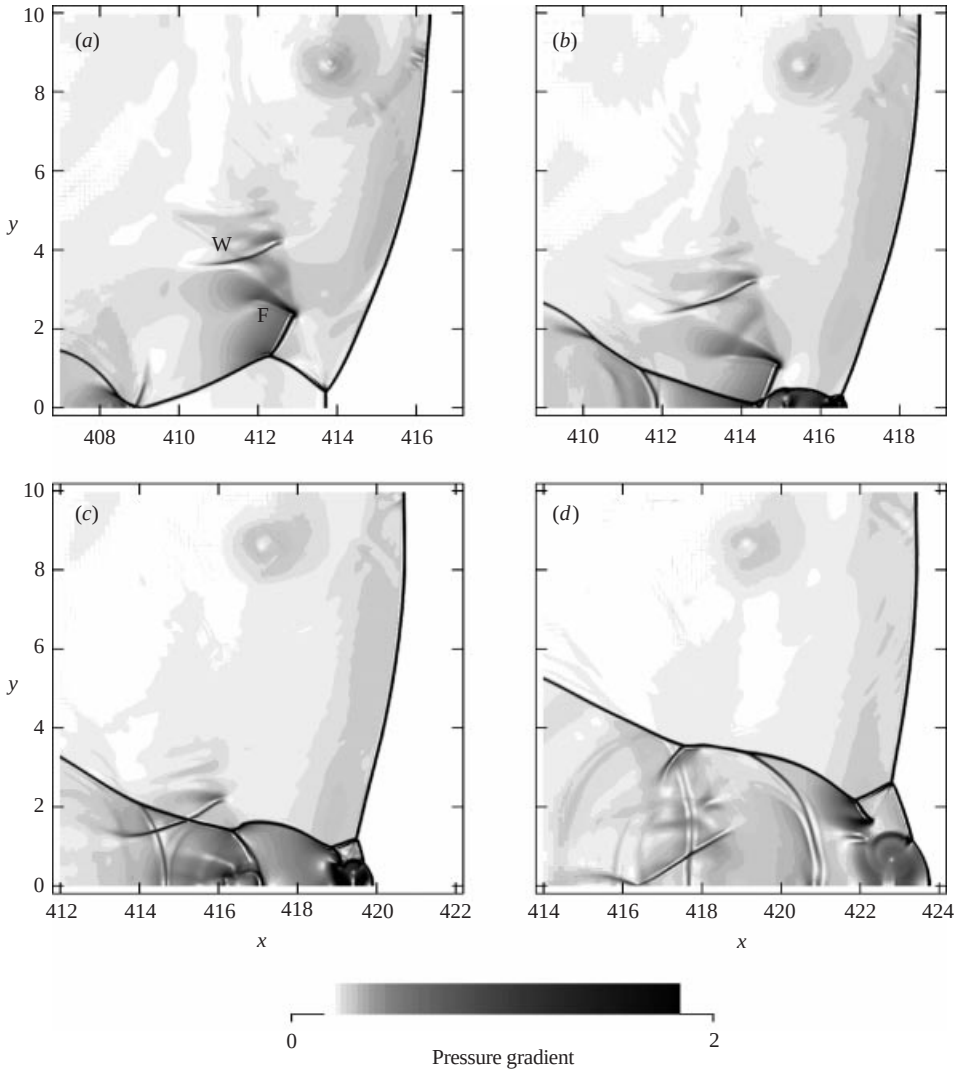

FIGURE 7. Pressure gradient for a resolution of 64 points/$l_{1/2}$ at times (*a*) 415.4, (*b*) 417.8, (*c*) 420.3 and (*d*) 423.3.

hence acting like a detonation itself. This shock wave formed shortly before $t = 415.4$ from a compression wave in the pocket of unburnt gas, which steepened into a shock and was then further strengthened by the heat release from the burning gas behind it. F is a rarefaction fan which is centred at point c.

By $t = 415.4$ the triple point a has travelled downwards and is just about to collide with the bottom boundary. Part of the transverse wave T in the region $x < 409$ has already collided and reflected from the boundary. Note that since a symmetry boundary condition is imposed at the bottom boundary, the transverse wave can be considered to be colliding either with a solid wall or with an identical transverse wave moving in the opposite direction. The Mach stem M has become very much weaker than at the earlier time of figure 1, resulting in much lower reaction rates and hence a much longer reaction length behind it. After collision and reflection of triple point

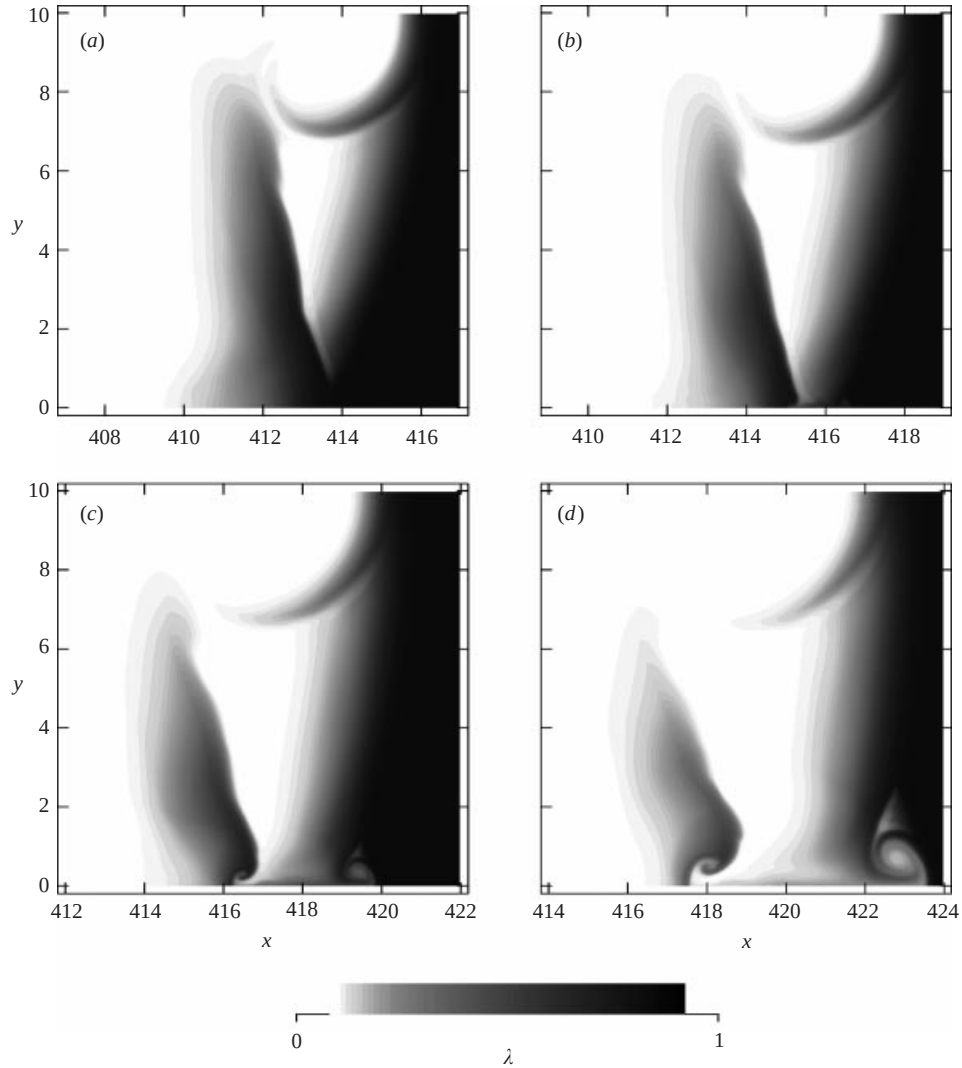

FIGURE 8. Reaction progress variable for a resolution of 64 points/$l_{1/2}$ at times (*a*) 415.4, (*b*) 417.8, (*c*) 420.3 and (*d*) 423.3.

a it becomes the incident shock. The small portion of the incident shock I remaining at $t = 415.4$ below triple point a is now very weak and the gas which has passed through it is burning very slowly.

When the triple point a collides with the bottom boundary it produces a region of very high temperature, dramatically increasing the reaction rate in the unburnt gas which had previously passed through the incident shock, causing an 'explosion within the explosion'. This hot and rapidly burning gas is squeezed along the boundary in a pair of forward and rear facing jets. As the jets spread they undergo a Rayleigh–Taylor-type instability, so that their heads develop into mushroom-like structures. The forward facing jet impacts on the new Mach stem, causing a portion of it to bulge outwards. Hence this interaction of the jet with the front is the origin of the kink in the Mach stem (cf. Quirk 1994). The new Mach stem is initially very strong.

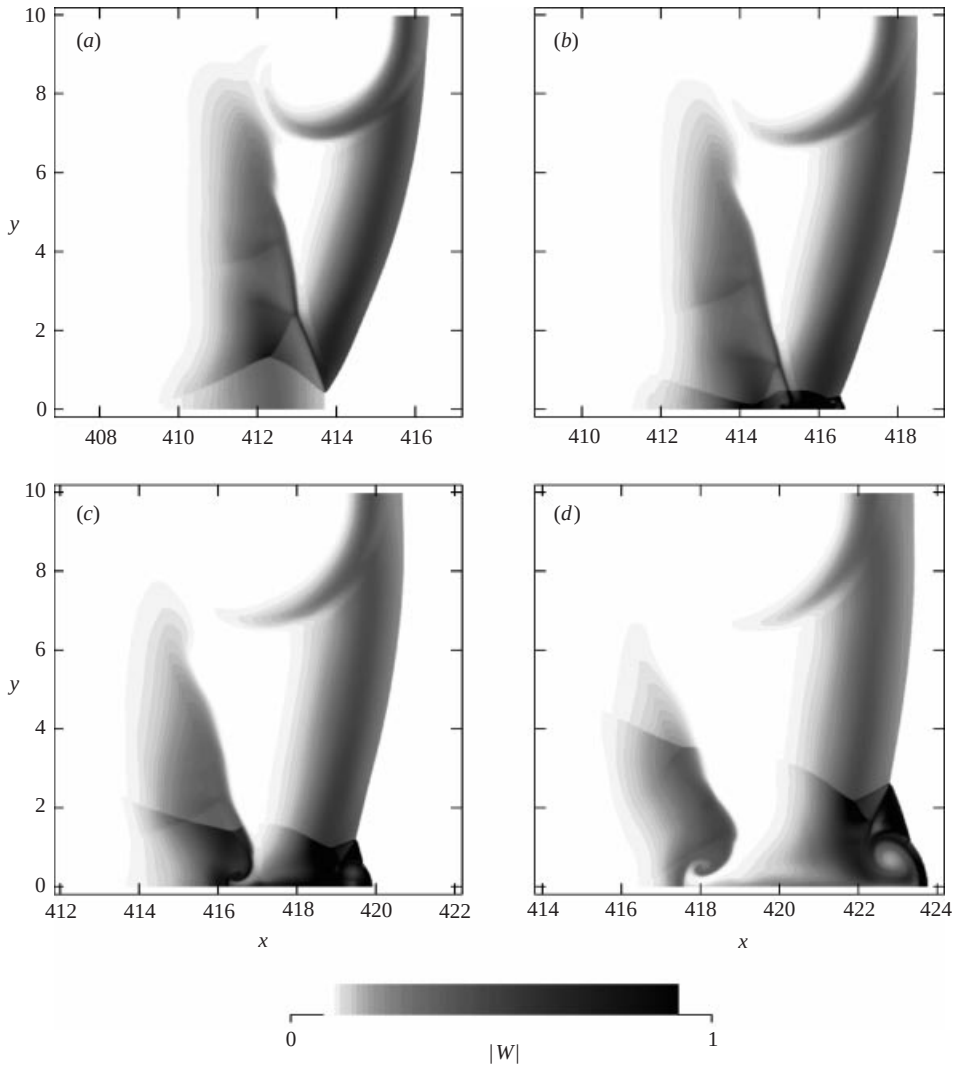

FIGURE 9. Reaction rate for a resolution of 64 points/$l_{1/2}$ at times (*a*) 415.4, (*b*) 417.8, (*c*) 420.3 and (*d*) 423.3.

Note that as the triple point collides the slip line S and the triple point configuration at b become detached from the front and begin to fall further and further behind it, creating a new unburnt pocket of fuel which is separated from the main reaction zone. The head of the rear facing jet then eats into this pocket.

A new double Mach configuration is subsequently created by the interaction of the jet with the Mach stem. A new slip line forms separating the gas passing through the new incident shock above the triple point from that passing though the Mach stem below it. This slip line then becomes rolled-up in the head of the jet. Note that the structure of the new double Mach configuration is very similar to that seen in the double Mach reflection case of an inert shock reflecting from a wedge (e.g. Glaz *et al.* 1985).

Note that many wave interactions and fine-scale details are involved in the triple point collision and reflection process, in a relatively small region. Hence it can be

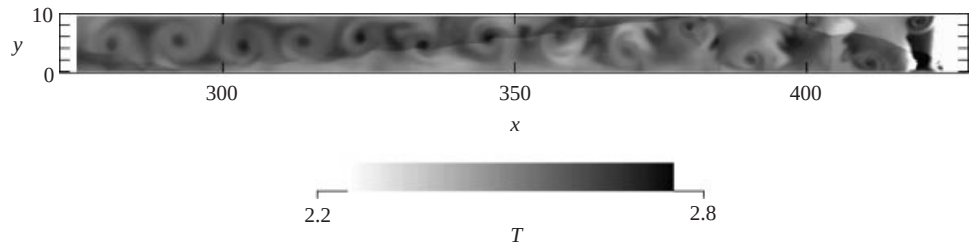

FIGURE 10. Temperature at $t = 423.3$ for a resolution of 64 points/$l_{1/2}$.

seen that very high resolution is required in the collision region to reveal the physical details in such a process.

Figure 10 shows the temperature at large distances behind the front. The series of transverse wave collisions produces a very inhomogeneous downstream temperature distribution. For reversible reactions with temperature-sensitive equilibrium compositions, this would produce very inhomogeneous products of burning. Note that the transverse wave can be seen to extend very far back (more than 100 half-reaction lengths) into the burnt gas.

6. Comparison with experiments and previous calculations

In this section, the results of the numerical simulations are compared with those of experiments and previous numerical calculations.

Strehlow & Crooker (1974) reconstructed the shock structures from schlieren photographs of cellular detonations in hydrogen–oxygen–argon mixtures. The numerically determined strong transverse shock structures shown here are in excellent agreement with figure 9 of Strehlow & Crooker (1974), including the triple points a and b, the slip line S, the detonation part of the transverse wave T and the location of the main reaction zones. The experiments of Strehlow & Crooker (1974) show that shortly after collision, a third triple point and associated slip line appears downstream of triple point b on the transverse shock, but they did not discuss its origin. This triple point recedes even further downstream from point b as the transverse wave propagates. The motion of this receding triple point writes a second track on the experimental soot plate, in addition to the track etched by points a and b (Strehlow & Crooker 1974). Such a second track is also seen in the numerical versions of the soot plate records (see Sharpe & Falle 2000*a*, where the second track was mistakenly identified as being due to the motion of the kink in the Mach stem, k). The results of § 5 reveal that this third triple point is actually the previous triple point b, along with its slip line, which became detached from the front during the collision process. It should be noted that at the time corresponding to figure 1, the triple point which was detached during the previous collision of the transverse wave with the upper wall has receded just downstream of the viewing window of the figure.

According to the qualitative picture of Strehlow & Crooker (1974), just after collision the shock structures appear to be quite simple and of the weak type, without any secondary triple points on the transverse wave, seemingly becoming of the strong type quite suddenly some time later. However, as pointed out by Fickett & Davis (1979), it is unclear what is happening just after collision in the experiments since the details are not resolved due to the very short space and time scales of both the reactions and the flow; nor can the experiments capture the very transient but very

high pressures and temperatures involved just after collision. The fact that numerical simulations can reveal details that cannot be determined in experiments is the main reason for performing such calculations. For example, the results of § 5 reveal the genesis of the triple points on the transverse wave. In contrast, the experiments suggest that the triple points appear suddenly out of nowhere, which is simply due to the fact that the experiments have so far been unable to capture the details of their birth. Indeed, the results of § 5 show that the structures involved just after triple point collision are much more complex than the experimental results suggest.

Strong transverse waves also appear in spinning detonations in tubes with circular cross-sections (Huang, Lefebvre & Van Tiggelen 2000, for example). In these cases the transverse wave rotates around the axis of the tube. Unlike the transverse waves seen in cellular detonation, however, a single spinning transverse wave propagates without change of structure as it never collides with a wall or another transverse shock. The structure of spinning transverse waves is still remarkably similar to transverse waves in cellular detonations when the triple points are far from collision (cf. figure 2 of Huang *et al.* 2000 with figure 1 of this paper).

The pockets of unburnt gas described in § 5 are also seen in the experiments. Subbotin (1975) presented a diagram of the locations of these unburnt regions of gas for detonations in hydrogen–oxygen–argon mixtures. Again, the results of § 5 are in excellent agreement with the qualitative results of the experiments (cf. figure 3 of Subbotin 1975 with figure 8 of this paper). Subbotin (1975) describes the pockets as triangular in shape with a characteristic notch at the vertex. The pocket of gas which can be seen to form in figure 8 is indeed roughly triangular in shape, and the numerics reveal that the notch at the vertex is actually due to the formation of the rear facing jet during the collision, which eats into the pocket. Indeed, the numerical simulations also reveal that the reason for the formation of the pocket of unburnt gas is the detachment of the slip line S during the triple point collision, as described in § 5. Note that the region of burnt gas entrained in the forward facing jet can also be seen in figure 3 of Subbotin (1975). The numerical results show that the head of the forward facing jet grows more quickly than that of the rear facing jet, which is again in agreement with the experimental results of Subbotin (1975).

Oran *et al.* (1982) considered the possible effects of the unreacted gas pockets. They suggest that if the pockets take a long time to burn out, the delay in their heat release could be sufficient that the detonation may eventually die out. Conversely, Oran *et al.* (1982) suggest that if the pockets burn out very quickly, then they could send out pressure pulses and even shocks that could overtake the front and strengthen it. Such pressure pulses are indeed seen when pockets of unburnt gas burn out quickly in numerical simulations of one-dimensionally unstable (pulsating) detonations (Sharpe & Falle 1999). In the present calculations, the compression wave which strengthens to shock W is produced by the burnout of the pocket at its edge. However, in this case the compression wave moves through the pocket itself, behind the slip line S and hence does not affect the shock front. Other compression waves produced by the later complete burning out of the pocket are left behind by the shock front and so do not affect it. The pockets burn out quickly enough so that the detonation continues to propagate in a self-sustained manner. Hence for the case considered in this paper, the pockets of unburnt gas are a result of the instability rather than being responsible for it, and appear to have little influence on the front.

Lefebvre & Oran (1995) performed numerical simulations in order to investigate transverse wave structures and found that the transverse wave is initially of the weak type (with no second triple point) just after collision but then becomes of the strong

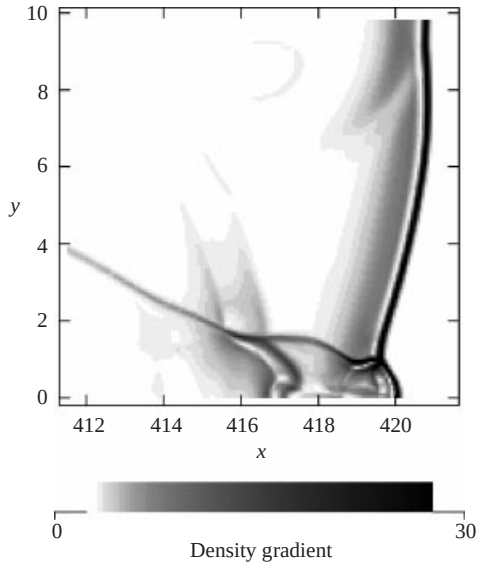

FIGURE 11. Density gradient for a resolution of 16 points/$l_{1/2}$ at $t = 421.0$.

type as it propagates, seemingly in agreement with the qualitative results of the experiments in Strehlow & Crooker (1974). While this may be due to the fact that Lefebvre & Oran (1995) use a reaction model representing dilute hydrogen and oxygen burning instead of the single irreversible reaction used in this paper, they only used about 12 points in the reaction zone. Our results show this is not enough to reveal or capture the events just after triple point collision, and hence suggest that Lefebvre & Oran's (1995) results are in agreement with the experiments simply because neither their calculations nor the experiments have sufficient resolution to capture the fine-scale, very transient details of the post-collision evolution. Figure 11, which shows the density gradient at a point in the cycle of reflections corresponding to figure 6(*c*), but for a resolution of just 16 points/$l_{1/2}$, demonstrates that this is indeed the case. For this lower resolution, it can be seen from figure 11 that none of the fine-scale physical details involved in the collision process are apparent. Importantly, the new triple point and shock structures produced in the collision are missing. Hence when such low resolutions are used, the transverse wave appears to be of the weak type just after collision, in contrast to the results for resolved calculations. Figure 11 is very similar to those in Lefebvre & Oran (1995) and hence we have reproduced their results and conclusions simply by using too coarse a numerical grid. It is important to note that this is not an issue of numerical method. If the numerical mesh spacing or timestep is of the order of, or larger than the physical scales, then the physical details will not be captured, regardless of the numerical scheme used. Resolutions of less than about 20 points/$l_{1/2}$ are simply too coarse to capture these details. The fact that numerical simulations can reveal details that cannot be determined in experiments is the main reason for performing such calculations. If, however, one does not properly resolve the flow in numerical simulations, then one has gained little more insight than the experiments provide.

The only other resolved calculation that we are aware of in the literature is that of Quirk (1994). He showed two snapshots of the temperature gradient just before and just after two triple points collide for a very high-resolution numerical simulation. Unfortunately, Quirk (1994) gave only a brief description of the details of the

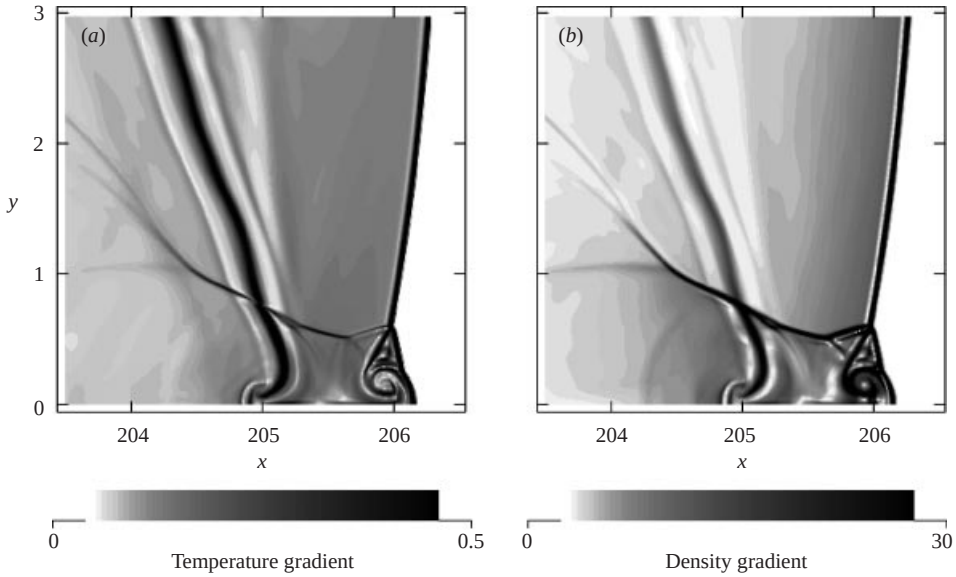

FIGURE 12. (*a*) Temperature and (*b*) density gradients for $E = 10$, $Q = 50$, $\gamma = 1.2$, $f = 1.2$ and $L = 5$ at $t = 205.9$. Resolution is 102.4 points/$l_{1/2}$

snapshots, because in that paper the author was concerned with the numerical issues involved with detonation simulations. Many of the features are in good agreement with our results, including the detachment from the front of the slip line, the forward and rear facing jets and the bulging and kinking of the Mach stem. There does, however, appear to be a qualitative difference between our results and those of Quirk (1994). In his figure 13, the new triple point configuration looks more like the complex Mach reflection situation of inert shocks reflecting from wedges (Glaz *et al.* 1985), with the bc type shock not apparent. However, Quirk (1994) used rather different parameters than we have. He considered two transverse waves, or one cell, in a channel of width 10, i.e. a cell size half that considered in this paper, for an overdriven detonation with degree of overdrive 1.2 and $E = 10$, $Q = 50$, $\gamma = 1.2$. Hence it appears that the parameter regime and cell size may have some influence on the nature of the collision processes and flow structures. In order to investigate this a simulation with the same parameter set as used by Quirk (1994) was performed; the same resolution as Quirk (1994), 102.4 points/$l_{1/2}$, was used (the results were also compared to a simulation with a resolution of 64 points/$l_{1/2}$ to ensure that the flow was resolved). While Quirk (1994) considered two transverse waves with a domain width of 10 and employed periodic transverse boundary conditions, in order to make the calculation less expensive, we used a domain width of 5 with reflective boundary conditions, with just one transverse wave. These conditions are identical as both represent transverse waves moving within a regular, repeating transverse wave spacing (or cell width) of 10 half-reaction lengths.

Figure 12 shows the results of the calculation. Figure 12(*a*), which shows the temperature gradient near the triple point shortly after collision, is in very good agreement with figure 13 of Quirk (1994), and in both cases it appears that for this parameter set the triple point collision is more like complex Mach reflection of inert shocks, with the bc shock not readily apparent, but with the slip line S, kinks in the transverse wave and Mach stem and forward and rear facing jets still present.

However, shock bc *is* clearly present in the plots of the density (and also pressure) gradient (figure 12*b*). Hence, while it is a relatively weak shock, bc is still present and the shock reflection is still actually like double Mach reflection. It is important to note that the cell size of 10 half-reaction lengths used in this calculation and that of Quirk (1994) is smaller than the natural cell size, which is usually between 20 to 50 steady reaction lengths (Lee 1984). As the cell size or transverse wave spacing increases the transverse wave strengthens (Sharpe & Falle 2000*a*).

7. Conclusions

In this paper, two-dimensional numerical simulations of a strong transverse wave in a detonation cell close to a natural cell size have been performed. Resolution studies show that in order to ensure that the transverse wave structure, motion and interaction with the burning are properly captured, more than 50 points/$l_{1/2}$ are required. For resolutions of less than about 20 points/$l_{1/2}$ it becomes difficult or impossible to correctly identify all the physical features of the flow and burning. At these lower resolutions, pockets of unburnt gas burn out much more quickly than for more resolved calculations. During triple point collision, fine scales and multiple wave interactions are involved, and hence very high resolutions are required. Low resolutions should not be used when such collision processes are important, such as in detonation diffraction problems, as we have shown that to do so leads to incorrect conclusions about the physical processes.

It is worth noting that Bourlioux & Majda (1992) employed front tracking instead of front capturing to track the lead shock. While they have shown that this offers several advantages for the initial stages of cell formation and at lower resolutions, even when the Mach stems and incident shocks are tracked, the transverse waves and various other discontinuities that appear in the flow must be captured. Hence high resolution is still required to capture them properly, and one still needs to resolve all the various (at times very short) reaction length scales involved in the problem.

The process of triple point collision was then examined using a resolution of 64 points/$l_{1/2}$. In this process a new pocket of burning gas is formed when the slip line becomes detached from the front. The double Mach configuration of the strong transverse wave also becomes detached and recedes from the front with the slip line. A new slip line and secondary triple point are formed from the reflection of the incident shock. The creation of a new Mach stem involves forward and backward facing jets which are Rayleigh–Taylor unstable, and the reflection process is very similar to that of double Mach reflection of inert shocks from a wedge.

In this paper, we have concentrated on a single parameter set and tube width, since our purpose has been to show the numerical issues involved with simulating cellular detonations, and what can be achieved by high-resolution calculations. However, in order to investigate how the transverse wave structure and evolution depends on the parameters or domain width, a calculation corresponding to that of Quirk (1994) was performed. The results are in good agreement with those of Quirk (1994), and in this case the collision process is still like double Mach configuration, with embedded jets and new slip lines still present, but the bc type of shock is much weaker shortly after the collision process. However, the dependence on the parameters and cell size still need to be investigated further and this will be addressed in a sequel.

Even though we have used a simple model with a single, irreversible reaction, the results of the numerical simulations are in remarkable agreement with experiments of real cellular detonations, including the transverse shock structures and nature of

the pockets of unburnt gas. However, it is known that, for detonations, qualitatively different chemical kinetics can produce qualitatively different results. For example Dold & Kapila (1991) have shown that the shock-induced ignition of detonations with a single reaction is different from that for detonations with three-step chain-branching kinetics. Hence the dependence of the flow and burning structures on the details of the chemical model used (e.g. chain branching models, the effect of reversibility, endothermic stages of reaction) needs to be investigated for cellular detonations. Short & Quirk (1997) have shown that for one-dimensionally unstable detonations with model chain-branching kinetics, the instability is qualitatively similar to the one-reaction case near the stability boundary, but differs from it for very unstable detonations in that for the chain-branching model the detonation has a definite detonability limit, whereas it does not for a single reaction (Sharpe & Falle 1999). However, Short & Quirk (1997) have also shown that substantially higher resolution can be required to obtain even the qualitatively correct solutions for more complex chemical models than for a single reaction, even in one dimension.

Our results are somewhat in disagreement with previous, low-resolution numerical simulations, such as those in Lefebvre & Oran (1995), but we find that we can reproduce their results when too coarse a numerical grid is used, demonstrating that this difference is simply due to the previous calculations being under-resolved.

While we have shown that it is possible to capture the salient features by using high-resolution calculations, the solutions of the Euler equations studied in this paper will not converge quantitatively, because smaller and smaller scales are resolved as the resolution decreases, since the artificial viscosity is grid dependent. For example, shock and flow discontinuity widths become thinner and thinner as resolution increases. Since cellular detonations involve slip lines which are unstable to the Kelvin–Helmholtz instability and jets which produce Rayleigh–Taylor-type instabilities, the evolution of these instabilities will also be grid dependent when the diffusional processes are. Indeed the only major difference between our results and those of Quirk (1994) is that the slip line is much more Kelvin–Helmholtz unstable in the calculations of Quirk (1994). This difference is due to the different flavours of the artificial dissipation in the two numerical schemes and whether or not slip lines and contacts are allowed to diffuse over a few grid cells or are artificially steepened. Since for Euler detonation simulations the evolution of the diffusive effects are grid and scheme dependent, such simulations may therefore be improved by solving the Navier–Stokes equations instead, with the inclusion of species diffusion and heat conduction. Such processes may have important effects, for instance in the relatively slowly burning pockets of fuel produced by transverse wave collisions. However, the viscosity would have to be set artificially high in order to resolve the viscous scales.

I am indebted to Mantis Numerics Ltd for the use of μCobra, and to Sam Falle for technical support. I would also like to thank the referees for suggestions which greatly improved the paper.

REFERENCES

Bourlioux, A. & Majda, A. J. 1992 Theoretical and numerical structure for unstable two-dimensional detonations. *Combust. Flame* **90**, 211–229.

Dold, J. W. & Kapila, A. K. 1991 Comparison between shock initiations of detonation using thermally-sensitive and chain-branching chemical models. *Combust. Flame* **85**, 185–194.

Falle, S. A. E. G. 1991 Self-similar jets. *Mon. Not. R. Astron. Soc.* **250**, 581–596.

Falle, S. A. E. G. & Giddings, J. R. 1993 Body capturing. In *Numerical Methods for Fluid Dynamics* (ed. K. W. Morton & M. J. Baines), vol. 4, pp. 337–343. Clarendon.

Falle, S. A. E. G. & Komissarov, S. S. 1996 An upwind scheme for relativistic hydrodynamics with a general equation of state. *Mon. Not. R. Astron. Soc.* **278**, 586–602.

Fickett, W. & Davis, W. C. 1979 *Detonation.* University of California Press.

Glaz, H. M., Colella, P., Glass, I. I. & Deschambault, R. L. 1985 A numerical study of oblique shock-wave reflections with experimental comparison. *Proc. R. Soc. Lond.* A **398**, 117–140.

Huang, Z. W., Lefebvre, M. H. & Van Tiggelen, P. J. 2000 Experiments on spinning detonations with detailed analysis of the shock structure. *Shock Waves* **10**, 119–125.

Lee, J. H. S. 1984 Dynamic parameters of gaseous detonations. *Ann. Rev. Fluid Mech.* **16**, 311–336.

Lefebvre, M. H. & Oran, E. S. 1995 Analysis of shock structures in a regular detonation. *Shock Waves* **4**, 277–283.

Oran, E. S., Young, T. R., Boris, J. P., Picone, J. M. & Edwards, D. H. 1982 A study of detonation structure: the formation of unreacted pockets. In *Nineteenth Symp. (Intl) on Combustion*, pp. 573–582. Pittsburgh: the Combustion Institute.

Quirk, J. J. 1992 A contribution to the great Riemann solver debate. *ICASE Rep.* 92-64.

Quirk, J. J. 1994 Godunov-type schemes applied to detonation flows. In *Combustion in High Speed Flows* (ed. J. Buckmaster, T. L. Jackson & A. Kumar), pp. 575–596. Kluwer.

Sharpe, G. J. 1997 Linear stability of idealized detonations. *Proc. R. Soc. Lond.* A **453**, 2603–2625.

Sharpe, G. J. & Falle, S. A. E. G. 1999 One-dimensional numerical simulations of idealized detonations. *Proc. R. Soc. Lond.* A **455**, 1203–1214.

Sharpe, G. J. & Falle, S. A. E. G. 2000*a* Two-dimensional numerical simulations of idealized detonations. *Proc. R. Soc. Lond.* A **456**, 2081–2100.

Sharpe, G. J. & Falle, S. A. E. G. 2000*b* Numerical simulations of pulsating detonations. Part I: nonlinear stability of steady detonations. *Combust. Theory Model.* **4**, 557–574.

Short, M. & Quirk, J. J. 1997 On the nonlinear stability and detonability limit of a detonation wave for a model three-step chain-branching reaction. *J. Fluid Mech.* **339**, 89–119.

Strehlow, R. A. 1969 The nature of transverse waves in detonations. *Astron. Acta.* **14**, 539–548.

Strehlow, R. A. & Crooker, A. J. 1974 The structure of marginal detonations. *Acta. Astron.* **1**, 303–315.

Subbotin, V. A. 1975 Two kinds of transverse wave structures in multifront detonations. *Combust., Explos., Shock Waves* **11**, 83–88.